Spectrochimica Acta Part A: Molecular and Biomolecular Spectroscopy 197 (2018) 37–42

Contents lists available at ScienceDirect

Spectrochimica Acta Part A: Molecular and Biomolecular Spectroscopy

journal homepage: www.elsevier.com/locate/saa

Design of tunable ultraviolet (UV) absorbance by controlling the Ag—Al co-sputtering deposition

Xin-Yuan Zhang [a,b], Lei Chen [c,d], Yaxin Wang [c], Yongjun Zhang [c], Jinghai Yang [a,b,c,*], Hyun Chul Choi [e], Young Mee Jung [d,*]

[a] Changchun Institute of Optics, Fine Mechanics and Physics, Chinese Academy of Sciences, Changchun 130033, PR China
[b] University of Chinese Academy of Sciences, Beijing 100049, PR China
[c] Key Laboratory of Functional Materials Physics and Chemistry of the Ministry of Education, Jilin Normal University, Changchun 130103, PR China
[d] Department of Chemistry, Institute for Molecular Science and Fusion Technology, Kangwon National University, Chuncheon 24341, Republic of Korea
[e] Department of Chemistry, Chonnam National University, Gwangju 61186, Republic of Korea

ARTICLE INFO

Article history:
Received 3 September 2017
Received in revised form 14 December 2017
Accepted 19 December 2017
Available online 20 December 2017

ABSTRACT

Changing the structure and composition of a material can alter its properties; hence, the controlled fabrication of metal nanostructures plays a key role in a wide range of applications. In this study, the structure of Ag—Al ordered arrays fabricated by co-sputtering deposition onto a monolayer colloidal crystal significantly increased its ultraviolet (UV) absorbance owing to a tunable localized surface plasmon resonance (LSPR) effect. By increasing the spacing between two nanospheres and the content of aluminum, absorbance in the UV region could be changed from UVA (320–400 nm) to UVC (200–275 nm), and the LSPR peak in the visible region gradually shifted to the UV region. This provides the potential for surface-enhanced Raman scattering (SERS) in both the UV and visible regions.

1. Introduction

In recent years, plasmonic nanomaterials have played a significant role in various fields, such as light harvesting, photocatalysis, sensing, surface-enhanced Raman scattering (SERS), and surface-enhanced fluorescence [1–11]. They have many novel properties in terms of optical, electromagnetic, and other aspects. Owing to these unique properties, a variety of studies have been conducted to prepare materials, varying their sizes, shapes, and other parameters to control their performance [12,13]. Noble metals, particularly Au and Ag, are used widely as plasmonic materials, and they have the ability to tune the localized surface plasmon resonance (LSPR) by controlling the material structure [14–16]. However, noble metals exhibit LSPR only in the visible and near-infrared (NIR) regions. Compared to tuning the red shift of LSPR, tuning of the blue shift has proven to be highly challenging [17].

Al is an ideal alternative substrate material for the blue shift of LSPR to the UV region, because the plasmonic frequency of Al is 13 eV, which is high enough to cause LSPR to occur in the deep-UV region (>6 eV) [18–20]. Moreover, the large imaginary part of the dielectric function, ε, of Al is beneficial for light harvesting; the stronger the near-field enhancement and ohmic damping of Al, the larger its absorption [21]. Recently, Al-based plasmonic materials have been investigated. Honda et al. successfully fabricated an Al nanostructure via oblique angle deposition and increased the reaction rate of UV photocatalysis owing to the LSPR effect [22]. Li et al. fabricated a 3D Al hybrid plasmonic nanostructure with large areas of hot spots and long-term stability via a millisecond laser direct writing method in liquid nitrogen and applied this in UV plasmon-enhanced spectroscopic sensing [23]. Taguchi et al. reported that by controlling the size of Al, the LSPR peak blue shifted from a wavelength of 340 nm down to 270 nm [14,24]. Moreover, Al is chemically active and thus, its outer layer can easily be oxidized to Al_2O_3 in the air, resulting in an SPR red shift [25]. This dense oxidized layer also protects the inner layer material from oxidization [17].

The structures of metal nanomaterials have been diversified during research into these materials. Template technology developed based on a monolayer colloidal crystal has provided an elastic way of preparing materials, whilst also ensuring the uniformity of the material structure [26]. The colloidal crystal array, cleaned by plasma, changes its size when the spacing between the metal particles is varied, affecting the properties of the entire material. In this study, we combined the specific properties of Ag and Al and used a magnetron sputtering method to prepare new nanocomposites with tunable UV absorbance. When the surface plasmon resonance effect of the two metals overlap with each other, it will produce the SPR energy transfer phenomenon, and realize the following tuning: (i) The nanosphere array will increase the optical path length of the scatter incident light in substrates, which increases the utilization of the light efficiently. (ii) This structure will concentrate

* Corresponding authors.
E-mail addresses: jhyang1@jlnu.edu.cn (J. Yang), ymjung@kangwon.ac.kr (Y.M. Jung).

https://doi.org/10.1016/j.saa.2017.12.056
1386-1425/

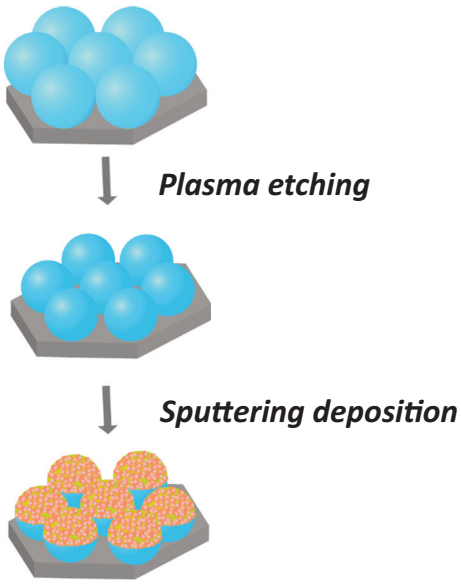

Fig. 1. The schematic of the fabrication process for Ag—Al ordered arrays.

incident light energy and provide to the SPR, which extends the light absorbed area. Additionally, both materials are highly abundant [27]. Ag has a tendency to be oxidized when exposed to the environment; however, after co-sputtering with Al, the outer Al layer will be rapidly oxidized to form an Al_2O_3 film barrier, which can guarantee the stability of the material. Al is an ideal UV-plasmonic material; it is advantageous for light harvesting, and its absorbance can be tuned from the visible to the UV region by the addition of Al to a Ag substrate. Therefore, a simple and controllable substrate for tuning absorbance from visible to UV light was studied [23,28,29].

2. Experimental Section

2.1. Materials

Ethanol (analytic reagent) and sodium dodecyl sulfate (analytic reagent) were purchased from Sigma-Aldrich Co., Ltd. Polystyrene (PS) colloid particles with a size of 200 nm (10 wt% aqueous solution) were purchased from Duke. Both Ag and Al targets with a purity of 99.99% were purchased from Beijing TIANRY Science & Technology Developing Center. H_2O_2 (30%) and NH_4OH (25%) were purchased from Sinopharm Chemical Reagent Co., Ltd. All the chemicals were used without further purification. Deionized ultrapure water (18.25 MΩ cm^{-1}) and silicon (Si) wafers were used throughout the present study.

2.2. Sample Preparation

Two-dimensional (2D) ordered monodisperse PS particles that are regarded as a template for metals were fabricated using self-assembly technology. To obtain a highly-ordered pattern, PS diluted in ultrapure water was tiled and then sodium dodecyl sulfate was added. The PS arrays were then removed by silicon wafers of size 2 × 2 cm^2 (more detailed methods for self-assembled PS can be found in our previous work) [30–33]. The spacing of neighboring nanospheres was changed in a plasmon cleaner (Model 1020, E.A. Fischione Instruments Inc.), and they were etched for 0, 30, 60, 90, and 120 s with the working gas (mixture of 80% O_2 and 20% Ar). The metal arrays on the PS were fabricated by a magnetron sputtering system (ATC 1800-F, USA AJA). The distance between the Ag and Al targets and substrates was 10 cm. The sputtering power of Ag was 20 W, while Al was sputtered at 20, 40,

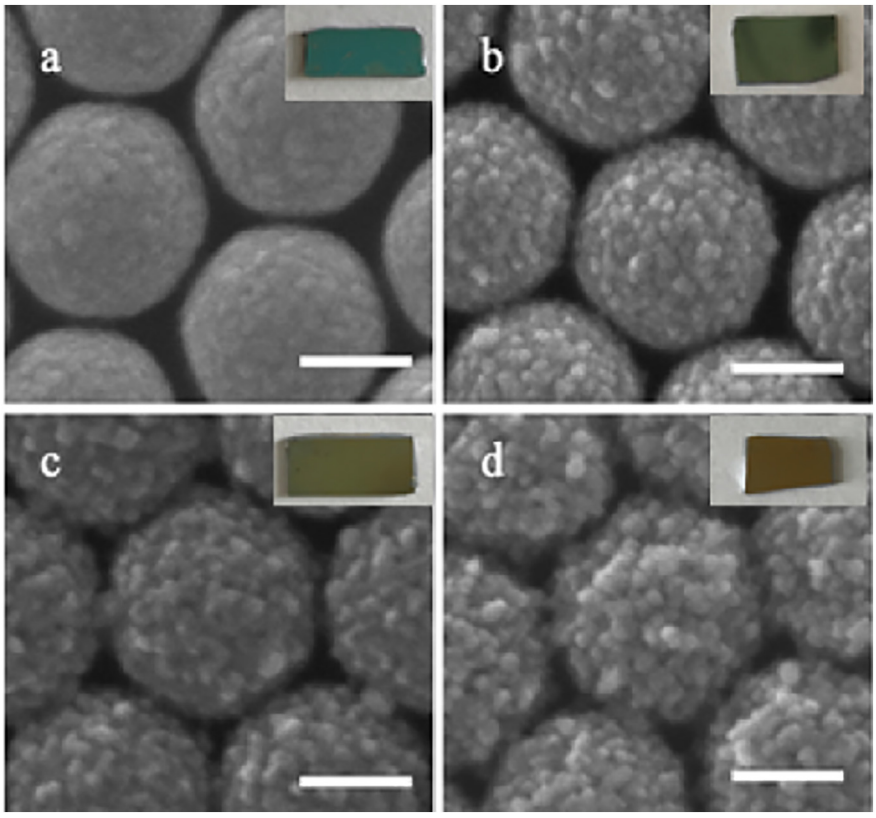

Fig. 2. SEM images of the Ag—Al ordered arrays, which consist of Ag, with a constant sputtering power (20 W), and Al, with varied sputtering powers, co-sputtered deposition for 300 s on the PS arrays without etching. The sputtering powers of Al were (a) 20 W, (b) 40 W, (c) 60 W, (d) 80 W, respectively (the insets are the corresponding optical photographs). All the scales above represent 100 nm.

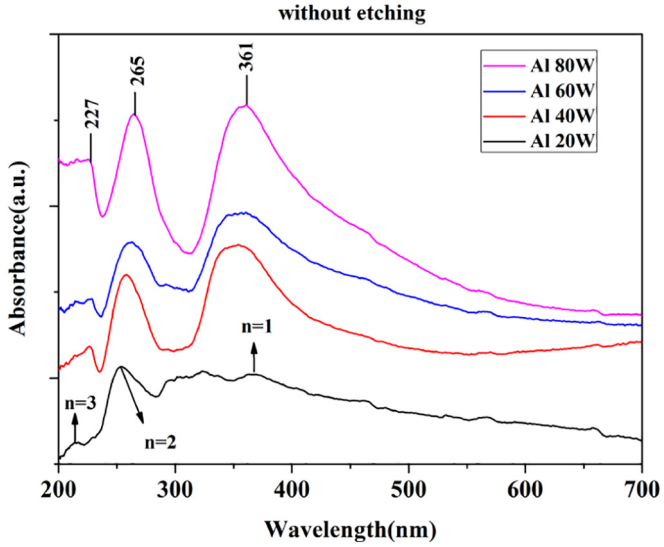

Fig. 3. UV–Vis absorbance spectra of Ag with a constant sputtering power (20 W), and Al with varied sputtering powers, (20 W, 40 W, 60 W, 80 W, separately), co-sputtered deposition for 300 s on the PS arrays without etching.

60, and 80 W, and co-sputtering deposition was carried out for 300 s with a working pressure of 5.8×10^{-3} Pa. Fig. 1 shows the schematic of the fabrication process of Ag—Al ordered arrays.

2.3. Characterization

To obtain the morphology and microstructure of the Ag—Al arrays, scanning electron microscopy (SEM) and transmission electron microscopy (TEM) images were obtained using a JEOL 6500F scanning electron microscope and a JEM-2100HR transmission electron microscope, respectively, operating at an accelerating voltage of 200 kV. Ultraviolet-visible (UV–Vis) absorption spectra were obtained using a Shimadzu UV-3600 spectrometer. X-ray photoelectron spectroscopy (XPS) was performed using a Thermo Scientific ESACLAB 250Xi A1440 system and the XPS spectra were calibrated using carbon (C 1 s = 284.6 eV). The analyzing spot size was 500 μm, using Al Kα radiation, and the energy step size was set at 1.0 eV.

3. Results and Discussion

It is well known that the roughness of particles affects the SPR of a substrate. Fig. 2 shows the SEM images of the Ag—Al ordered arrays, which consist of Ag, with a constant sputtering power (20 W), and Al, with varying sputtering powers (20, 40, 60, and 80 W), co-sputtered for 300 s on the PS arrays without etching (the insets of Fig. 2 are the corresponding optical photographs). As shown in Fig. 2, as the sputtering power of Al increases, the grain sizes change from ~12 to ~24 nm, increasing the roughness of the substrate surface and changing the optical colors.

Fig. 3 shows the corresponding UV–Vis absorbance spectra of the Ag—Al ordered arrays. Three local SPR peaks at approximately 361, 265, and 227 nm are observed, which are the dipole ($n = 1$), quadrupole ($n = 2$), and octupole ($n = 3$) resonances, respectively [16]. As shown in Fig. 3, as the sputtering power of Al increases, the absorbance peaks are red shifted. Such a red shift is mainly due to the increasing content of Al. As we know, dielectric constant is a frequency-dependent quantity that causes the change of the plasmon response, and can be expressed as

$$\varepsilon_{(\omega)} = \varepsilon'_{(\omega)} + j\varepsilon''_{(\omega)} \quad (1)$$

here, the imaginary part $\varepsilon_{(\omega)}''$ represents dielectric loss. In generally, after the surface is oxidized, the positive dielectric constant will be higher, and absorbance red shift will occur. The thickness of the oxide

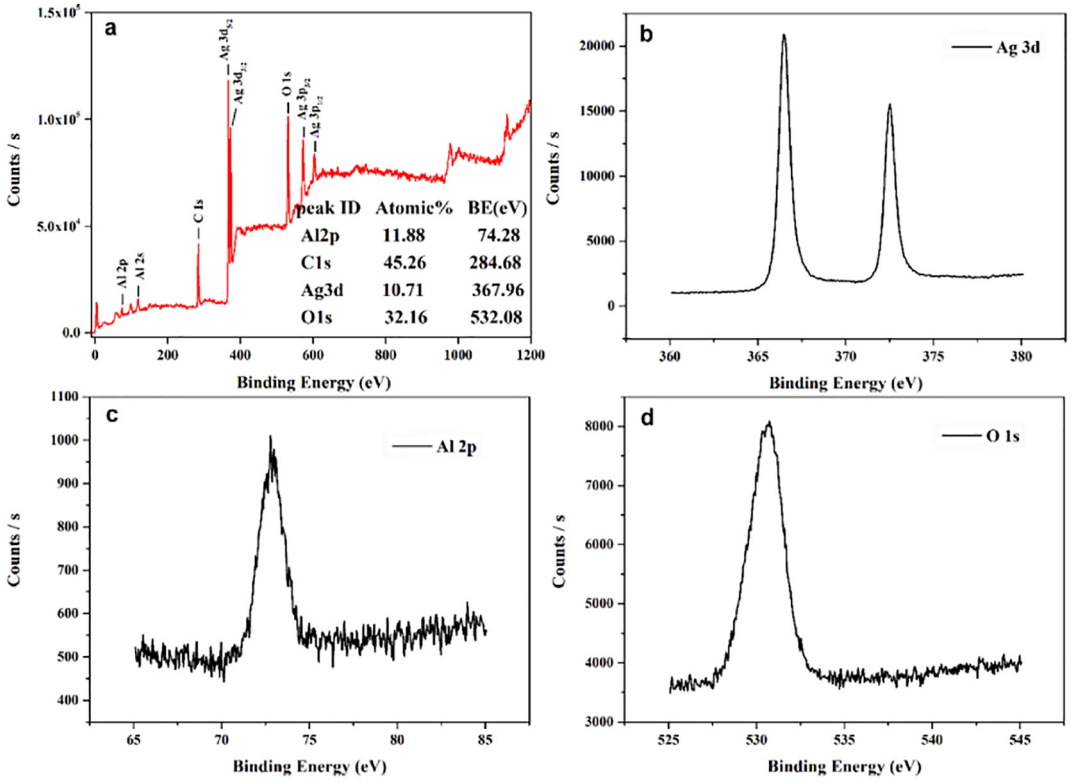

Fig. 4. (a) The XPS survey spectrum of Ag (20 W sputtering power) and Al (20 W sputtering power) co-sputtered deposition for 300 s on the PS arrays without etching, and Ag 3d (b), Al 2p (c), and O 1 s (d) XPS spectra.

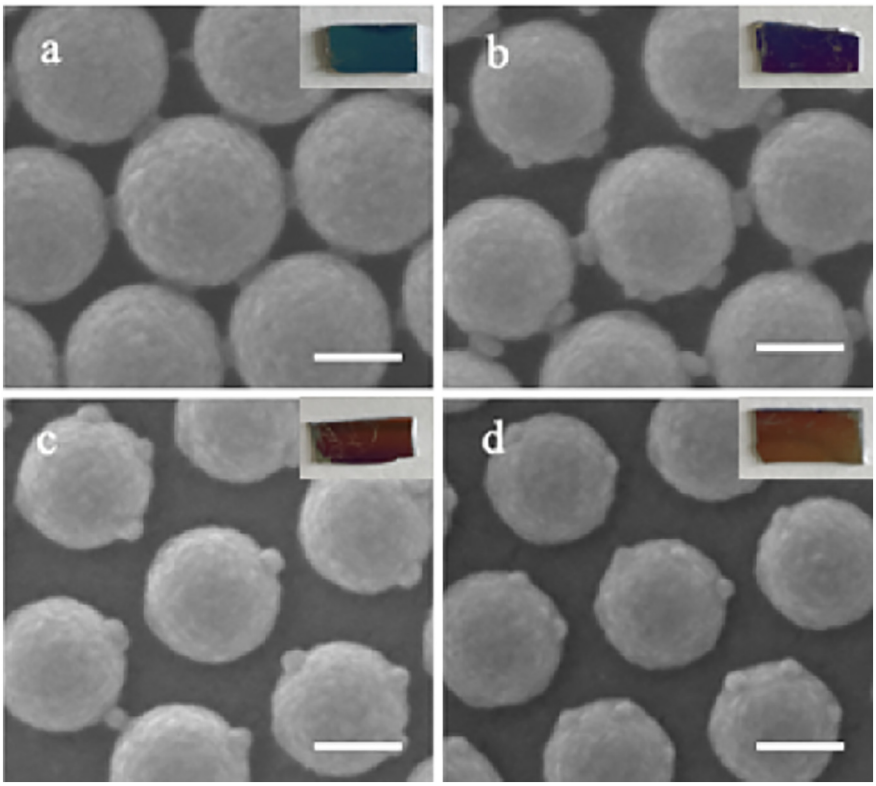

Fig. 5. SEM images of the Ag—Al ordered arrays, which consist of Ag (20 W sputtering power) and Al (20 W sputtering power) co-sputtered deposition on the PS arrays with etching for (a) 30 s, (b) 60 s, (c) 90 s, and (d) 120 s, respectively (the insets are the corresponding optical photographs). All the scales above represent 100 nm.

layer as an essential factor also determines the degree of shift. So, as the sputtering power of Al increases, the thickness of Al_2O_3 increases, leading to the absorbance red shift. This is in good agreement with recent reports [25]. The size and roughness of the particles also affect the red shift. For a quantitative analysis of the relationship between the content of Al_2O_3 and the wavelength of absorbance, XPS is of considerable importance. As shown in Fig. 4, all the peaks are shifted owing to the electrostatic charging of the surface layer. The binding energies in the XPS spectra presented in Fig. 4 are calibrated using carbon (C 1 s = 284.6 eV). Fig. 4(a) illustrates the XPS survey spectrum of the Ag—Al ordered array with Ag (20 W sputtering power) and Al (20 W sputtering power) co-sputtered deposition for 300 s on the PS arrays without etching, suggesting that it is covered with Al, Ag, C, and O. The C peak (C 1 s = 284.6 eV) is assigned to an adventitious carbon-based contaminant, and the binding energies of Al 2p, Ag 3d, and O 1 s of the Ag—Al ordered array are 74.28, 367.96, and 532.08 eV respectively. Fig. 4(b) shows the peaks of Ag $3d_{5/2}$ and Ag $3d_{3/2}$ at 368.10 and 373.40 eV, respectively, which can be indexed to Ag [34]. In the Al 2p XPS spectrum shown in Fig. 4 (c), the peak at 74.10 eV can be assigned to Al_2O_3, which means that the Al on the surface of the sample has been oxidized [20]. In the O 1 s XPS spectrum, a peak at 531.08 eV was observed. The XPS spectra demonstrated that the Al on the surface of the sample was oxidized, not the Ag. This is because the Ag was protected after the Al was oxidized to Al_2O_3, guaranteeing the stability of the material.

The size of particles also affects the SPR of the substrate. After the co-sputtered deposition of Ag (20 W sputtering power) and Al (20 W sputtering power) using a magnetron sputtering system for 300 s on the PS arrays with different etching times, the substrate colors are significantly different. After etching for 30, 60, 90, and 120 s, the colors of the substrates were blue-green, deep purple, pink, and bronze,

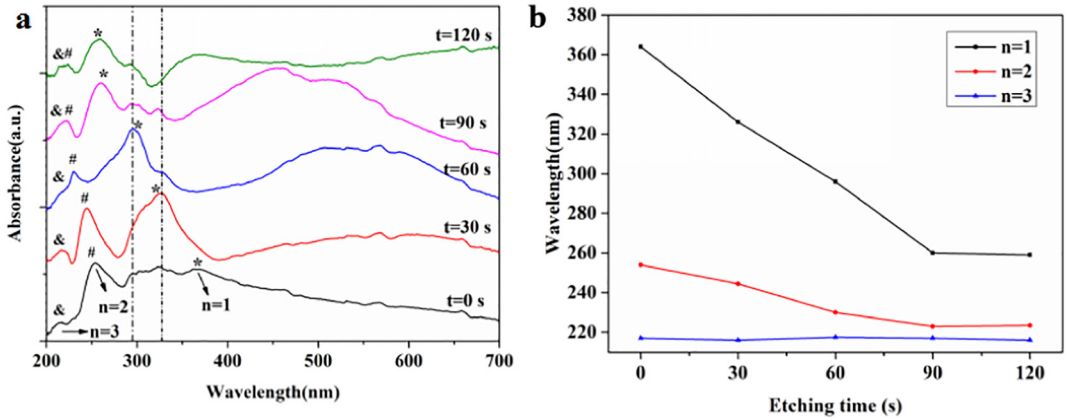

Fig. 6. (a) UV–Vis absorbance spectra of Ag (20 W sputtering power) and Al (20 W sputtering power) co-sputtered deposition for 300 s on the PS arrays with different etching times (t). (b) The chart showing the relationship between wavelength and etching time in different resonance modes.

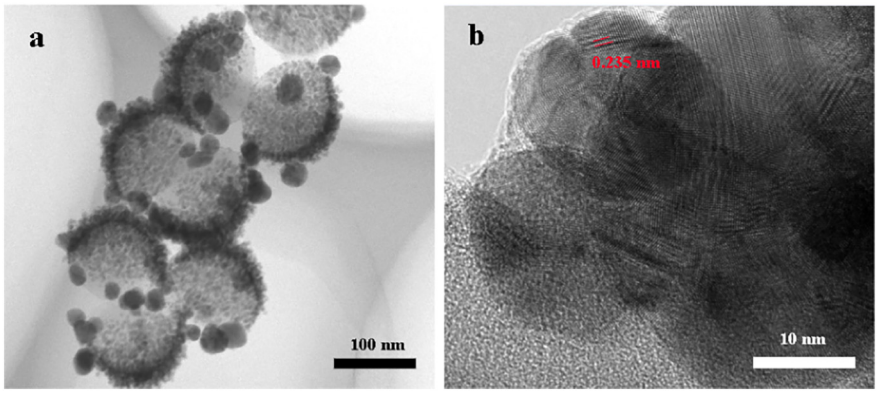

Fig. 7. TEM images of the Ag—Al ordered arrays, which consist of Ag with sputtering power (20 W) and Al (sputtering power 80 W) co-sputtered deposition for 300 s on the PS arrays and etching for 90 s.

respectively; the SEM images are shown in Fig. 5 (the insets are the corresponding optical photographs). As illustrated in the SEM images, with an increasing etching time in the plasmon cleaner, the sphere sizes decrease from 200 nm to 140 nm. The PS spheres become isolated when they are etched for 90 s, as shown in Fig. 5(c) and their color is different. We examined the SPR using the absorbance spectra, shown in Fig. 6(a). The dashed lines at ~300 and ~330 nm correspond to the single atom absorbance and dipole resonance peaks of Ag [35], respectively, and some of them are coupled with the resonance peaks of Al; this coupling broadens the absorbance of the substrate. The marked peaks are the multi-resonance peaks of Al; the nanoparticle sizes are small enough so that the three valence electrons of the Al atom keep a rare high electron density, leading to multi-resonance. The marks correspond to dipole ($n = 1$), quadrupole ($n = 2$), and octupole ($n = 3$) resonances, separately [17]. When the time of etching was increased from 0 to 90 s, the dipole and quadrupole resonances are conspicuously blue shifted, while the octupole resonance changed only slightly. As we know, absorption curves can provide structure information of the substrate. Here, the absorbance on the red side of 350 nm is the SPR of two materials. After etching for 30 s, with the curvature of PS is increased and the size is decreased, the broad peak appeared. And with an increasing etching time, the SPR peaks are blue shifted. The analysis of the relationship between the etching times and the wavelength of the maximum absorbance is shown in Fig. 6(b). The wavelength changed linearly with the etching time before etching for 90 s. This is because the arrays seem to be isolated after etching for longer than 90 s; the optical color and the absorbance also changed slightly.

Fig. 7 shows the TEM images of the Ag—Al ordered array, formed by co-sputtering Ag (20 W sputtering power) and Al (80 W sputtering power) for 300 s on the PS arrays and etching for 90 s. The structure looks like caps and is obviously grainy, which is in good agreement with the SEM images. After etching, the size of the 2D ordered monodisperse PS colloid particles is approximately 140 nm and there are plenty of larger grains, as shown in Fig. 7(a). The high-resolution TEM image in Fig. 7(b) exhibits the lattice fringe. The spacing of the lattice fringe was 0.235 nm, which can be attributed to the (111) plane of Ag, indicating that Ag nanoparticles formed and were well-crystallized, while the Al_2O_3 around the Ag was amorphous.

This array, which could be used for controlling the absorbance of the material in the UV region has many advantages: (i) both the elements used are abundant in nature, and Al is very cheap; (ii) the method of fabrication is easy enough for large-scale production; (iii) although Ag has a tendency to be oxidized, after co-sputtering with Al, the outer Al will be rapidly oxidized to Al_2O_3, which forms a film barrier that will protect the Ag from oxidation, guaranteeing the stability of the material; (iv) the near-field enhancement and ohmic damping of Al are strong, increasing its absorption, making it beneficial for light harvesting; by adding Al to the Ag substrate, the absorbance can be tuned from the visible to the UV region. Therefore, we have provided a simple, steady, and controllable solution for tuning absorbance from the visible to UV region.

4. Conclusion

We have successfully controlled the UV absorbance of an Ag—Al array by tuning the spacing of the spheres and the content of Al via co-sputtering deposition onto a monolayer colloidal crystal. As the spacing and the Al content are increased, the UV absorbance is tuned owing to the tunable LSPR effect. This enables us to couple with UV light and widen the application of SERS in the UV and visible regions. After co-sputtering of Al and Ag, the outer Al rapidly oxidizes to Al_2O_3 and acts as a film barrier to prevent the Ag from oxidizing, thereby guaranteeing the stability of the material. The inherent properties of Al as an ideal UV-plasmonic material promote light harvesting, and using Ag as a traditional SERS substrate is beneficial for Raman detection. Therefore, the new material can be used to study UV-SERS.

Acknowledgements

This work was supported by the National Natural Science Foundation of China (No. 61775081, 61575080, and 61405072), Program for the development of Science and Technology of Jilin province (No. 20150519024JH, and 20150520015JH), and Technology of Education Department of Jilin Province (No. 2016-217). This work was also supported under the framework of international cooperation program managed by the National Research Foundation of Korea (No. NRF-2017K2A9A2A06014372).

References

[1] H.A. Atwater, A. Polman, Nat. Mater. 9 (2010) 205–213.
[2] K. Aydin, V.E. Ferry, R.M. Briggs, H.A. Atwater, Nat. Commun. 2 (2011) 517.
[3] S. Linic, U. Aslam, C. Boerigter, M. Morabito, Nat. Mater. 14 (2015) 567.
[4] N. Liu, M. Mesch, T. Weiss, M. Hentschel, H. Giessen, Nano Lett. 10 (2010) 2342.
[5] S. Ostovarp, L. Rocks, K. Faulds, D. Graham, V. Parchansky, P. Bour, E.W. Blanch, Nat. Chem. 7 (2015) 591.
[6] F. Nicoli, D. Verschueren, M. Klein, C. Dekker, M.P. Jonsson, Nano Lett. 14 (2014) 6917.
[7] J. Bochterle, F. Neubrech, T. Nagao, A. Pucci, ACS Nano 6 (2012) 10917–10923.
[8] R. Thomas, R.S. Swathi, J. Phys. Chem. C 116 (2012) 21982–21991.
[9] L. Chuntonov, G. Haran, Nano Lett. 13 (2013) 1285–1290.
[10] L. Chen, Y. Zhao, Y. Wang, Y. Zhang, Y. Liu, X.X. Han, B. Zhao, J. Yang, Analyst 141 (2016) 4782–4788.
[11] L. Chen, Y. Zhao, Y. Zhang, M. Liu, Y. Wang, X. Qu, Y. Liu, J. Li, Colloids Surf. A Physicochem. Eng. Asp. 507 (2016) 96–102.
[12] W. Li, Y. Qiu, L. Zhang, L. Jiang, Z. Zhou, H. Chen, J. Zhou, Biosens. Bioelectron. 79 (2016) 500.
[13] M.J. Mcclain, A. Schlather, E. Ringe, N.S. King, L. Liu, A. Manjavacas, M.W. Knight, I. Kumar, K.H. Whitmire, H.O. Everitt, P. Nordlander, N.J. Halas, Nano Lett. 15 (2015) 2751.

[14] A. Taguchi, Y. Saito, K. Watanabe, S. Kawata, Appl. Phys. Lett. 101 (2012) 081110–081114.
[15] H. Yokota, T. Taniguchi, T. Watanabe, D. Kim, Phys. Chem. Chem. Phys. 17 (2015) 27077–27081.
[16] T. Ghodselahi, T. Neishaboorynejad, S. Arsalani, Appl. Surf. Sci. 343 (2015) 194–201.
[17] J. Hu, L. Chen, Z. Lian, M. Cao, H. Li, W. Sun, N. Tong, H. Zeng, J. Phys. Chem. C 116 (2012) 15584–15590.
[18] A. Ahmadivand, S. Golmohammadi, Opt. Laser Technol. 66 (2015) 9–14.
[19] J.M. Sanz, D. Ortiz, R.A.D.L. Osa, J.M. Saiz, F. Gonzalez, A.S. Brown, M. Losurdo, H.O. Everitt, F. Moreno, J. Phys. Chem. C 117 (2013) 19606–19615.
[20] M.W. Knight, N.S. King, L. Liu, H.O. Everitt, P. Nordlander, N.J. Halas, ACS Nano 8 (2014) 834–840.
[21] Y.C. Chung, P.J. Cheng, Y.H. Chou, B.T. Chou, K.B. Hong, J.H. Shih, S.D. Lin, T.C. Lu, T.R. Lin, Sci. Rep. 7 (2017) 39813.
[22] M. Honda, Y. Kumamoto, A. Taguchi, Y. Saito, S. Kawata, J. Phys. D. Appl. Phys. 48 (2015) 184006.
[23] X.M. Li, M.H. Bi, L. Cui, Y.Z. Zhou, X.W. Du, S.Z. Qiao, J. Yang, Adv. Funct. Mater. 27 (2017) 1605703.
[24] J. Zhu, J.J. Li, J.W. Zhao, Appl. Surf. Sci. 314 (2014) 145–150.
[25] L. Zhou, Y. Tan, J. Wang, W. Xu, Y. Yuan, W. Cai, S. Zhu, J. Zhu, Nat. Photonics 10 (2016) 393–398.
[26] G. Liu, Y. Li, G. Duan, J. Wang, C. Liang, W. Cai, ACS Appl. Mater. Interfaces 4 (2011) 1–5.
[27] Q. Hao, C. Wang, H. Huang, W. Li, D. Du, D. Han, T. Qiu, P.K. Chu, Sci. Rep. 5 (2015) 15288.
[28] L. Zhou, C. Zhang, M. Mcclain, A. Manjavacas, C.M. Krauter, S. Tian, F. Berg, H.O. Everitt, E.A. Carter, P. Nordlander, N.J. Halas, Nano Lett. 16 (2016) 1478–1484.
[29] P.M. Schwab, C. Moosmann, M.D. Wissert, E.W.G. Schmidt, K.S. Ilin, M. Siegel, U. Lemmer, H.J. Eisler, Nano Lett. 13 (2013) 1535–1540.
[30] Y. Wang, X. Zhao, C. Lei, S. Chen, M. Wei, M. Gao, Y. Zhao, C. Wang, X. Qu, Y. Zhang, J. Yang, Langmuir 30 (2014) 15285–15291.
[31] Y. Zhang, C. Wang, J. Wang, L. Chen, J. Li, Y. Liu, X. Zhao, Y. Wang, J. Yang, Spectrochim. Acta A 152 (2016) 461–467.
[32] Y. Wang, C. Yan, L. Chen, Y. Zhang, J. Yang, Nano 7 (2017) 159.
[33] Y. Wang, X. Zhao, W. Gao, L. Chen, S. Chen, M. Wei, M. Gao, C. Wang, Y. Zhang, J. Yang, RSC Adv. 5 (2015) 7454–7460.
[34] C. Zhao, B. Li, J. Du, J. Chen, Y. Li, J. Alloys Compd. 691 (2016) 772–777.
[35] T. Gong, J. Zhang, Y. Zhu, X. Wang, X. Zhang, J. Zhang, Carbon 102 (2016) 245–254.